Tikrit Journal of Engineering Sciences

TJES Tikrit Journal of Engineering Sciences

Open Access

Article

Improving the Dynamic Performance of Hybrid Storage Systems Provided by PV Solar Panels

Mohammed Albaker Najm Abed [1]*, Ali Abdul Razzaq Altahir [2], Ahmed Abdulhadi Al-Moadhen [2]

[1] Department of Computer Technology Engineering, Al Taff University College, Karbala, 56001, Iraq.
[2] Department of Electrical and Electronics Engineering, University of Kerbala, Karbala, Iraq.

Emails:
Mohammed Albaker Najm Abed: e09163265@s.uokerbala.edu.iq, Ali Abdul Razzaq Altahir: ali.altahir@uokerbala.edu.iq ,
Ahmed Abdulhadi Al-Moadhen: ahmedh1333@uokerbala.edu.iq

Abstract:

Solar energy is a clean, renewable resource receiving much attention as a competitive alternative to conventional energy sources. The subject of this study is the integration of rechargeable batteries, supercapacitors, and photovoltaic panels into a hybrid storage system. These parts work together to improve system performance and overcome the shortcomings of individual technologies. Supercapacitors' high power density and fast charge-discharge times enhance the energy density of rechargeable batteries. The battery's lifespan is increased, and adding a supercapacitor enhances the system's overall dynamic performance. The supercapacitor improves the operating conditions of batteries and photovoltaic panels by buffering current variations. The DC-DC converter design and the selection of the maximum power point tracking (MPPT) algorithm significantly impact the system's performance. This study examines the performance of several DC-DC converters, such as the boost and Super-lift Luo converters, and analyzes several MPPT techniques. The supercapacitor is essential when determining which combination suits a given set of operating conditions. An energy management system has been designed to synchronize the charging and discharging of the PV panels, supercapacitor, and battery. Optimal power flow and practical energy storage are ensured by a bidirectional DC-DC converter controlled by a fractional-order proportional-integral-derivative controller. The simulation results show that the Super-lift Luo converter outperforms the boost converter in terms of efficiency and power delivery. The perturbation-and-observation algorithm produces a peak power output of about 980 watts by efficiently tracking the PV panels' highest power point. The energy management system efficiently balances the energy distribution between the battery, supercapacitor, and load to ensure optimal system functioning. This study demonstrates how hybrid storage devices can effectively capture solar energy. A viable way to address the growing need for clean, sustainable energy is to combine the benefits of PV panels, supercapacitors, and rechargeable batteries. It is evident that when utilizing a super lift Luo, the battery's state of charge is approximately 0.2% greater than when using a boost converter. Additionally, super lift Luo is higher for supercapacitors, reaching 0.4% more significantly than a boost converter. The battery and supercapacitor can be charged faster and more efficiently due to the higher efficiency and power output of the HESS employing a super-lift Luo converter.

Keywords:

Artificial Neural Networks; Boost converter; Enhanced Particle Swarm Optimization; Energy Management System; Incremental Conductance; Perturbation and Observation; Super lift-Luo converter.

Highlights:

- Hybrid system combines batteries and supercapacitors for optimal PV storage.
- Bidirectional DC-DC converter ensures stable voltage and efficient energy flow.
- Supercapacitors handle rapid load changes to extend battery lifecycle.
- PI control strategy maintains DC bus stability under varying solar radiation.
- Dynamic performance improved through coordinated energy management.

Citation:

Abed MAN, Altahir AA, Al-Moadhen AA. **Improving the Dynamic Performance of Hybrid Storage Systems Provided by PV Solar Panels**. *Tikrit Journal of Engineering Sciences* 2026; **33**(1): 2155.

Article History:

Received:	24	Apr.	2024
Received in revised form:	15	Sep.	2024
Accepted:	19	Apr.	2025
Final Proofreading:	19	Apr.	2026
Available online:	14	May	2026

https://doi.org/10.25130/tjes.33.1.22

Corresponding Author*:

Mohammed Albaker Najm Abed
Department of Computer Technology Engineering, Al Taff University College, Karbala, 56001, Iraq.
Email:e09163265@s.uokerbala.edu.iq

1.INTRODUCTION

In recent years, clean energy sources, including PV panels, wind, and fuel cells, have been used to meet the enormous energy demand. PV systems and solar thermal applications generate electricity for heating, cooling, and other purposes. PV-based applications can be employed in grid-tied, standalone, or hybrid generating modes in conjunction with other renewable energy sources, such as HEV. They comprise numerous separate solar cells, most of which are silicon-based. Sunlight causes electrons in solar cells to break free from their atoms. These electrons produce an electric current as they move through the cell. The cell generates more electricity as it receives more sunshine. Reducing greenhouse gas emissions, which contribute to climate change, can be achieved using PV panels to generate power [1]. Using PV panels to charge SC and batteries and choosing battery types and suitable methods, such as the MPPT algorithm, charge controller, and DC-DC converter, is essential to achieve high efficiency in extracting and using electric power [2]. One standard tool for describing the performance of solar systems is the voltage-power curve (P-V). It contains a point known as the maximum power point, which indicates the highest energy output of the PV system. Should the characteristic curve be stationary, the PV system should be able to be controlled to achieve the MPP for the duration of its life. On the other hand, under real-world conditions, the characteristic curve varies nonlinearly with environmental factors such as solar radiation and PV cell temperature. They were making it difficult to obtain the MPP. These problems are resolved by using MPPT techniques. Any solar system aiming to get the most energy from its PV panels needs to track the best power. Numerous methods are used for maximum power extraction, including Perturbation and Observation [3], the fuzzy logic technique [4], incremental conductance [5], and practical swimming optimization [6]; any further methods can be found in the literature [7]. This paper will use the modern PSO algorithm, named after the enhanced PSO MPPT algorithm. Also, P&O should be used to improve this method into a flexible step-size P&O technique. Using a specified number of solar power measurements, an artificial neural network (ANN) method identifies the PV array's global maximum power point. All previous MPPT algorithms will be compared based on maximum power extraction, efficiency, and effects on the charging operation. Battery provision is required in the proposed HESS. In grid-tied mode, the battery absorbs extra electricity and delivers stored energy. Batteries and supercapacitors supply peak and off-peak power in a standalone application such as a hybrid electric vehicle (HEV) [8]. Batteries are not the only energy source used in modern energy storage systems; ESSs are battery-based [9]. The battery's power density must be high enough to deliver the required peak power. However, they cost more than their equivalents with a lower power density [10]. There are still batteries available with higher power densities. While they are accessible, batteries with a higher power density are significantly more costly than those with a lower power density. If a HEV's regeneration brakes are used to feed this excess directly into the battery without any control, the battery's lifetime could decrease [11]. Thermal management makes it difficult for rechargeable batteries to operate securely under heavy load situations. The system is built because of the technique, and before the battery, the supercapacitor charges and discharges. Assume that the grid frequency stays below the predetermined minimum even after the supercapacitor has been entirely depleted, as the supercapacitor begins to charge. In that case, the battery will discharge, extending its lifespan [12]. The main objective of using a DC-DC converter with a solar panel is to regulate and match the PV panel's voltage to the battery voltage; it uses the optimal voltage to obtain the maximum current to charge the battery [13]. The typical boost, buck, among the varieties of DC-DC converters are buck-boost converters. This paper will compare a super *lift-Luo* and a boost converter and their effects on the PV panel. When hybrid energy storage is utilized, DC-DC converters are required; they have a specific architecture. The DC-DC converter in HESS controls the energy storage system's charge and discharge operations. When charging, it functions as a low-to-high-voltage buck converter, and when discharging, it acts as a high-to-low-voltage boost converter for low voltage [14]. A HESS that combines PV panels, batteries, and supercapacitors offers several advantages for residential, commercial, and industrial applications. HESS can lower peak loads and increase overall system efficiency by storing excess energy generated by PV panels during peak sunshine hours and discharging it during high-demand periods. HESS contributes to grid stabilization and lowers voltage and frequency variations by balancing the supply and demand for electricity. HESS can provide reliable backup power during grid outages, ensuring critical system uptime and minimizing downtime. Greater energy independence and lower energy prices can result from HESS's ability to lessen reliance on the grid. Supercapacitors can quickly deliver and absorb power, making HESS ideal for voltage control and frequency regulation that require quick reaction times. Batteries can withstand fewer charging and discharging cycles by sharing the load with supercapacitors, thereby increasing their total longevity.

Intelligent control systems that maximize efficiency and save costs by optimizing energy storage and use can be installed on HESS. Applications for HESS include off-grid power systems, electric car charging, and integration of renewable energy sources. Using photovoltaic systems and energy storage, HESS may lower greenhouse gas emissions and advance sustainable development. By enhancing grid resilience and stability, HESS can lower the chance of blackouts and poor power quality. The following plan summarizes the current study: Section two methodology includes (MPPTs algorithm, PV-panel, SC, battery, DC/DC converter, and EMS); while in section three, results and discussion have been presented; and section four shows the conclusions and remarks.

2.METHODOLOGY

2.1.*Maximum Seeking Power Controllers*

A maximum-seeking solar controller is a device that optimizes the power extracted from PV panels. It does this by matching the solar panels' electrical impedance to the battery bank or the grid. That allows the solar panels to run at their MPP for a given set of conditions, resulting in increased power output from the solar system [15].

2.1.1.Perturbation and Observation Controller

Because of its simple implementation, the most frequently used approach is the perturbation and observation algorithm. As the names indicate, it depends on the system's disturbance caused by a rise or reduction in reference voltage, which directly affects the chopper converter's cycle, and then monitors the effects on the panel's output power. As power increases, the duty cycle also changes similarly. It is approaching the maximum point. Therefore, if there is a power failure, it goes away from the MPP. The duty cycle variation must then be reversed in a direction [16, 17].

2.1.2.Enhanced Particle Swarm Optimization

The suggested MPPT algorithm, a hybrid of Levy flight optimization (LFO) and PSO, and hereafter referred to as enhanced particle swarm optimization (EPSO), will eliminate mutual drawbacks to achieve more effective MPP search performance. PSO is initially used as a checking algorithm in the proposed EPSO approach to determine the MPP [1]. After identifying the global maximum, LFO will take over and operate at that point to improve accuracy. Adding a duty cycle constraint varies the suggested LPSO technique from the traditional PSO. This constraint checking is added for every duty cycle before updating location and velocity [18, 19].

2.1.3.Artificial Neural Networks

A system with an artificial neural network is one whose architecture first drew inspiration from the schematic operation of biological neurons before shifting more toward statistical techniques. An arrangement of connected cells, known as neurons, makes up an artificial neural network. In parallel, each neuron operates independently of the others, building a system that determines which tasks are essential to accomplishing functions. Instead of programming, learning techniques are used to construct the network and process the information it receives [20]. Figure 1 shows the MPPT control (based on neural networks) that operates on the photovoltaic system. Temperature (T) and radiation (G) are atmospheric data used as input variables for the MPPT command, with the duty cycle (D) of the output controlling how best to operate the converter.

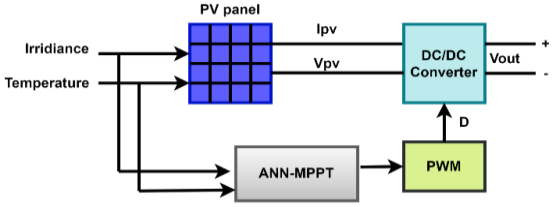

Fig. 1 ANN-MPPT System Block Diagram.

Appropriately learning artificial neurons is necessary for a neural controller to work efficiently. Levenberg-Marquardt was the algorithm used for training. 70% of the 100 data sets are used, 15% are allocated to testing, 15% to validation, and 15% for training. Finding the network structure is one issue that needs to be fixed before using a neural network. Three layers have been selected for this work: an input layer with two neurons, one for measuring surface temperature and the other for measuring solar irradiance, and ten neurons in a hidden layer. A single neuron in the output layer provides the duty cycle [21].

2.1.4.Incremental Conductance Controller

Conductance and incremental conductance can be used to determine the operating point at the maximum power point. Thus, to follow the MPP, one can compare the immediate and the incremental conductance. The duty cycle will increase if the instantaneous conductance exceeds the opposite of the incremental conductance. Assuming this does not occur, the duty cycle will be reduced. The block's subsystem used the PV's input voltage and current modules to compute the variations in conduction angle [22].

2.2.Photovoltaic Panel

The specifications of the PV panel in this research are given in Table 1 below: The solar field comprises parallel and series modules to achieve the required power. Every module consists of individual cells [23]. A single-diode model balances simplicity and accuracy well, making it ideal for this research. Regarding the PV panel's mathematical model, built in the

MATLAB-Simulink environment, a one-diode model, as shown in Fig.2, was considered [24].

Table 1 Technical Specifications Concerning PV Panels.

Variable	Value
Parallel strings	4
Series-connected	2
Highest Power	120.7 W
Cells per module	72 cell
O.C voltage	21 V
S.C current	8 A
MPP voltage	17 V
IMPP	7.1 A

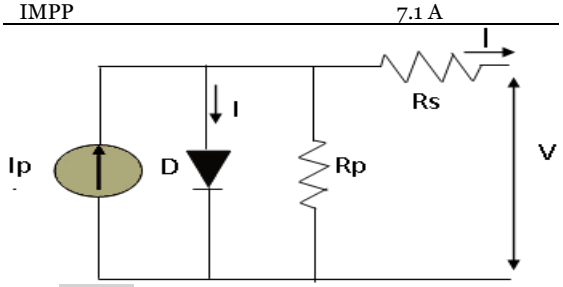

Fig. 2 Equivalent Circuit of PV Panel.

The model was created using the following Eq.(1) [18]:

$$I_{ph} = [I_{sc} + K_I(T_c - T_{ref})]\frac{G}{G_{ref}} \quad (1)$$

The current at the junction is expressed as follows:

$$I_d = I_s(\exp(\frac{q(V + R_s I)}{N.K.T} - 1) \quad (2)$$

The following gives the current flowing through the resistance Rsh:

$$I_{sh} = \frac{(V+R_s I)}{R_{sh}} \quad (3)$$

Hence,

$$I = [I_{sh} + K_I(T_c - T_{ref})]\frac{G}{G_{ref}} - I\left[\exp\left(\frac{q(V+R_s I)}{N.K.T}\right) - 1\right] - \frac{(V+R_s I)}{R_{sh}} \quad (4)$$

The output current will rise in response to increased solar radiation, increasing the extended power (P-PV). The irradiance is measured in units of W/m^2. Equation provides the mathematical relationship between Equations power, current, and irradiance (5).

$$\frac{G1}{G2} = \frac{I_2}{I_1} = \frac{P_2}{P_1} \quad (5)$$

Most solar panel outputs are assessed under standard test conditions. This is stated at 25 C°, or 77 F. Therefore, the PV panel's output voltage and power drop as the temperature rises. Here are a few techniques used in hot and cold climates to manage PV panel temperature changes.

$$V_T = \frac{kT}{q} \times nI \times N_{cell} \quad (6)$$

where: I_d is the diode current; I_{sc} is the current at a short circuit;I_o is the diode saturation current;I_1, I_2 are the solar panel's currents; I_s is the diode's reverse saturation current; V_d is the diode voltage; Rs is the diode's series resistance; R_{sh} is the diode's parallel resistance (Ω); V_{pv} is the voltage across the diode;P_1, P_2 are the power of the solar panel; T is the junction's Kelvin cell temperature; nI is the diode ideality factor; Ki is the temperature coefficient of the short-circuit is the (1.602×10-19 C); N is the ideality issue of the diode;N_{cell} is the number of cells in a module connected in series; G1 and G2 are the solar irradiance of the PV panel [25].

2.3.Battery Mathematical Model

The charger device can recharge the battery packs externally from the power grid. The battery is a critical component widely used in applications that depend on HESS, like hybrid and electric vehicles (EVs) (HEVs). Fig.3 depicts the battery's analogous circuit [26].

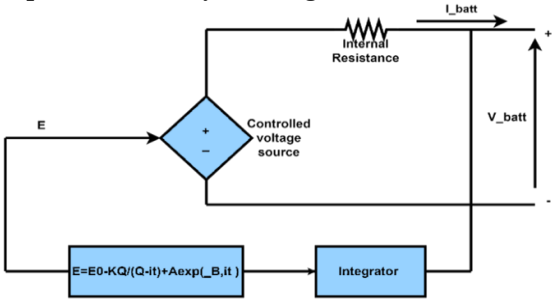

Fig. 3 Rechargeable Batteries Equivalent Circuit.

Equation (7) describes the battery voltage V_{bat} and provides the controlled voltage source.

$$V_{bat} = E - R_{bat}I_{bat} \text{ , and } E = E_o - K\frac{Q}{Q_D - \int i.dt} + A.exp(-B\int i.dt) \quad (7)$$

where E is the voltage when there is no current; E_o is the battery's potential constant; K is the potential of polarization; Q is the capacity of the battery's storage; A is the exponential zone's value (V); B is the inverted exponential zone time constant (Ah)-1. The technical specifications of the rechargeable battery in this study are given in Table 2:

Table 2 Technical Specifications Concerning Battery.

Variable	Value
Rated voltage	24 V
Nominal capacity	14 Ah
Percentage state of charge	50%
Battery response time	0.1 sec.

2.4.Mathematical Model for Supercapacitor

One of the newest developments in energy storage, particularly for embedded devices, is SC. The SC is a support and protection device for the battery [19]; it can handle sudden overloads in the system due to its characteristics. SC is used in HESS with the battery to extend the battery's lifecycle. Fig.4 below shows the SC electrical model. The model consists of an analogous series of resistances. R_{SC} connected in series with a capacitance C_{SC}. Eq.(8) provides SC voltage V_{UC} as a function of SC's current I_{UC} and SC power. Table 3 shows the supercapacitor parameters used in the HESS [27].

$$V_{SC} = V_I - R_{SC} * I_{SC} = \frac{Q_{SC}}{C_{SC}} - R_{SC} * I_{SC} \text{ , and } P_{SC} = \frac{Q_{SC}}{C_{SC}} * I_{SC} - R_{SC} * I_{SC^2} \quad (8)$$

where Q_{SC} is the amount of energy that is stored within a cell.

Employing a storage component called an SC, which comprises many cells coupled in parallel and series, respectively, by Ns and Np. Eq.(9) defines the SC stack's capacity and resistance.

$$C_{SC} = C_{elem}\frac{N_p}{N_s} \text{ , and } R_{SC} = R_{elem}\frac{N_s}{N_p} \quad (9)$$

Given the element voltage and current, the stack's voltage and current are given by Eq.(10).

$$V_{SC} = N_s.V_{elem} \text{ , } I_{SC} = N_p.I_{elem} \quad (10)$$

Table 3 Technical Specifications of Supercapacitor.

Variable	Value
Nominal Condenser	29 F
Series fighting	0.003 Ω
Nominal voltage	32 V
Number of series capacitors	1
Parallel capacitors	1
Initial potential	32V
Working temperature	$25C^o$

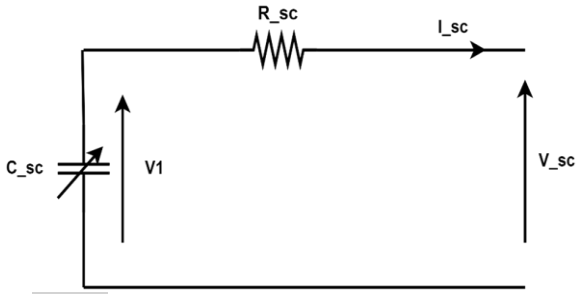

Fig. 4 Super Capacitor Equivalent Circuit.

2.5.*Chopper Converter*

The PV module and the electrical load are connected via a chopper converter. It is often used in DC power sources, such as DC drives and photovoltaic panels, to achieve the required voltage by converting uncontrolled DC input to controlled DC output. It is likely to regulate the voltage from the solar system by storing the input energy in the transformer's inductance for a short while, then releasing it to the output at a variable voltage. Those are effective converters (88.20-96.55%). Several DC-DC converter types are employed with PV panels. This paper presents a simple comparison of the proposed super *lift-Luo* and boost converters.

2.5.1.*Super-Lift LUO Converter*

New step-up (boost) converters from DC to DC, employing the voltage lift technique, were developed from prototypes in several models. These converters have simple construction, increased power density, high efficiency, and an inexpensive topology for positive-to-positive DC-DC voltage-raising conversion. The *lift-Luo* converter produces lower output-voltage ripples and a higher potential gain than the boost converter. Based on its capabilities, the Luo converter is categorized as a Super-Lift converter and a voltage-lift converter. The lift-Luo converter's passive architecture includes two diodes, a capacitor, and an inductor. Discusses the various Luo converters, as given in [28, 29]. The super lift Luo converter can function effectively by keeping to the following premise:(1) The resistance to the load (R_{output}) needs to be high. (2) The switching time must have a time limit. (3) Capacitors Cs_1 and Cs_2 need to have high values. (4) The duty ratio (d) value must be low. Eq.(11) provides the voltage gain equation for the super lift-*Luo* circuit.

$$G_s = \frac{V_{output}}{V_{input}} = (\frac{2-\delta}{1-\delta})^n \quad (11)$$

V_{output} and V_{input} are, respectively, the super-lift Luo circuit's input and output voltages. The Gain G_s Depends on the number of stages (n) and the duty ratio (δ). When switch Q is in the off position, V_{input} is the input voltage used to charge the capacitor C_{s-1}. Concurrently, as the inductor current $I_{L_{-1}}$Discharges, there is a slight voltage drop ΔV_{Cs-1}. When the inductance $I_{Ls_{-1}}$ value is high, one considers the average inductor current (Ls-1). Eq.(12) gives the voltage across the capacitor (C_{s-1}) and the capacitor voltage when the converter switches from off to on state, with the transition state set to the on state.

$$V_{cs\_1} = V_{input} - \Delta V_{Cs-1} \text{ , } \Delta V_{Cs\_1} = \frac{1}{C_{s-1}}\int_{\delta T}^{T} I_{L_{s-1}}dt = \frac{1-\delta}{C_{s-1}} T I_{L_{s-1}} \quad (12)$$

Equation (13) provides the total current flowing through the inductor and capacitor, which is the input current during turn-on and provides the input current as the current flowing through the inductor and capacitor when switch Q is open and the input current during the off-time.

$$I_{input\_on} = I_{C_{s-1-on}} + I_{L_{s\_1\_on}} \text{ , and } I_{input\_off} = I_{C_{s-1-off}} + I_{L_{s\_1\_off}} \quad (13)$$

The equations estimate the output current, a dependent parameter that depends on the capacitor's duty ratio and current Eqs. (14-15).

$$\delta T I_{C_{s\_1\_on}} = (1-\delta) T I_{C_{s\_1\_off}} \text{ , } I_{input\_off} = I_{C_{s-1-off}} = I_{L_{s\_1}} \text{, and } I_{C_{s-1-on}} = \left(\frac{1-\delta}{\delta}\right) I_{L_{s-1}} \quad (14)$$

$$I_{input\_on} = I_{L_{s\_1}} + \left(\frac{1-\delta}{\delta}\right) I_{L_{s-1}} = \frac{I_{L_{s\_1}}}{\delta} \quad (15)$$

The total input current in the on and off states relative to the duty ratio is the average input current.

$$I_{input} = \delta I_{input\_on} + (1-\delta) I_{input_{off}} \quad (16)$$

$$\frac{V_{input}}{I_{input}} = (\frac{1-\delta}{2-\delta})^2 \frac{V_{output}}{I_{output}} = (\frac{1-\delta}{2-\delta})^2 R_{output} \quad (17)$$

Equation (18) gives the output voltage ripple as a function of the resistance (R_{output}) and the capacitor (C_{s-2}).

$$\Delta V_{output} = \frac{I_{output}(1-\delta)T}{C_{s-2}} = \frac{(1-\delta)V_{output}}{fC_{s-2}R_{output}} \quad (18)$$

Raising C_{s-2}reduces the ripple voltage to a minimum. Capacitor C_{s-1}has a higher value than a capacitor C_{s-2}, which is made feasible using duty ratio d values smaller than unity. Equation (19) provides the error formula for the output voltage of the super_lift Luo converter.

$$e_{Super\_lift\ Luo} = V_{Dc-ref} - V_{Dc-Super\_lift\ Luo} \quad (19)$$

Where is the $e_{Super\_lift\ Luo}$ is the Super_lift Luo converter's error, $V_{Dc-ref}$is the converter's desired output.is the converter's desired output, and $V_{Dc-Super\_lift\ Luo}$ is the Super_lift Luo converter's output voltage.

2.5.2.Boost Converter

The conventional boost converter has a wide range of applications in power electronic applications, such as solar power systems and controlled DC power supplies. Increasing the desired load's DC output voltage from a low DC input voltage is beneficial. There are two current operating modes for the converter. There are two types of current modes: continuous (CCM) and discontinuous (DCM) (CCM). The traditional boost converter can function at multiple power levels and in any current mode in power applications, and every setting has unique variation features [30, 31]. The specifications of the boost and super-lift Luo converter in this study are given in Table 4.

Table 4 Technical Specifications of the Boost and Super-Lift Luo Converter.

Variable Name	Numerical Value
Input capacitance	3500*10^{-6} F
Output Capacitance	570*10^{-5} F
Inductance	100*10^{-6} H
R-load	5 Ω

The diode is reverse-biased when the switch is closed. Kirchhoff's voltage law is applied around the path, including the closed switch, inductor, and source, as given in Eq. (20).

$$v_L = V_s = L\frac{di_t}{dt} \quad (20)$$

The current change in the inductor is calculated from Eq.(21).

$$\frac{\Delta i_L}{\Delta t} = \frac{\Delta i_L}{\delta T} = \frac{V_s}{L} \quad (21)$$

Finding the value of Δi_Lwhile the switch is closed,

$$(\Delta i_L)_{closed} = \frac{V_s\,\delta T}{L} \quad (22)$$

When the switch opens, the diode becomes forward-biased, providing a channel for the inductor current that prevents it from changing instantly. The voltage across the inductor is constant when the output voltage:

$$v_L = V_s - V_o = L\frac{di_L}{dt} \quad (23)$$

Since the inductor current changes constantly, it must vary linearly when the switch opens. The following is how the inductor current varies when the switch is open:

$$\frac{\Delta i_L}{\Delta t} = \frac{\Delta i_L}{(1-D)T} = \frac{V_s - V_0}{L} \quad (24)$$

when calculating Δi_L,

$$(\Delta i_L)_{open} = (V_s - V_0)\frac{(1-\delta)T}{L} \quad (25)$$

From Eqs. (22-25), there must be no net change in inductor current to achieve steady-state operation.

$$(\Delta i_L)_{closed} + (\Delta i_L)_{open} = \frac{V_s\delta T}{L} +$$
$$(V_s - V_0)\frac{(1-\delta)T}{L} = 0 \Rightarrow V_o = \frac{V_s}{1-\delta} \quad (26)$$

I_L By calculating the average inductor current and using various substitutes, this can be expressed as follows in Eq. (27):

$$I_L = \frac{V_s}{(1-\delta)^2 R} = \frac{V_o^2}{V_s R} = \frac{V_o I_o}{V_s} \quad (27)$$

The average value of Eq.(27-28) and the variation in current are used to calculate the maximum and minimum inductor currents.

$$I_{max} = I_L + \frac{\Delta i_L}{2} = \frac{V_s}{(1-\delta)^2 R} + \frac{V_s\delta T}{2L}, \text{ and}$$
$$I_{min} = I_L - \frac{\Delta i_L}{2} = \frac{V_s}{(1-\delta)^2 R} - \frac{V_s\delta T}{2L} \quad (28)$$

In the boost converter, the lowest feasible combination of switching frequency and inductance for continuous current is so. It is helpful to express L in terms of a desired Δi_L, value, from a design standpoint, that is given in Eq. (29).

$$L_{min} = \frac{\delta(1-\delta)^2 R}{2f}, L = \frac{V_s\delta T}{\Delta i_L} = \frac{V_s\delta}{\Delta i_L f} \quad (29)$$

with the switching frequency denoted by f. As an alternative, capacitance is the ripple in the output voltage. An expression for ripple voltage is given in Eq. (30).

$$\frac{\Delta V_o}{V_o} = \frac{\delta}{RCf} = C = \frac{\delta}{R\left(\Delta V_o / V_o\right) f} \quad (30)$$

Eq. (31) provides the voltage ripple induced by the ESR and the corresponding error formula.

$$\Delta V_{o,ESR} = \Delta i_c r_c$$
$$= I_{L,max} r_C, \text{ and } e_{boost}$$
$$= V_{DC-ref} - V_{DC-boost} \quad (31)$$

Where is the e_{boost} is the boost converter's error, $V_{DC-ref}$is the converter's desired output.is the converter's desired output, and $V_{DC-Boost}$ is the boost Converter's output voltage [32].

2.5.3.Bidirectional DC-DC Converters

The bidirectional DC-DC converter's objective is energy management systems (EMS). Power density, cost, weight, and reliability are critical factors for bidirectional power flow, such as in electric vehicles. Bidirectional DC/DC converters (BDCs) are more efficient, need fewer parts, and are less expensive. They are commonly used to control charge and discharge operations. Figure 5 presents a schematic representation of the bidirectional DC-DC converters used in this concept. Note that separate bidirectional DC-DC converters are included in the supercapacitor and the rechargeable battery. Switches 1 and 2 in the converter switch the output when specific logic conditions are met. The PI controllers instruct switches S1 and S2 to turn ON and OFF by the

controller duty cycle during charge and discharge operations [33].

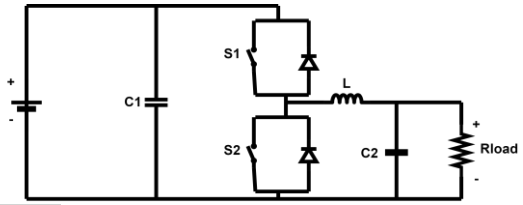

Fig. 5 Hybrid Energy Storage System (HESS) with a DC-DC Converter Operating in Both Directions.

2.6.Energy Management System

Three PI Controllers generate a control signal to adjust the energy distribution between the battery, the solar PV supply, and the supercapacitors. It ensures the most effective energy distribution, considering the system's power needs and the unique characteristics of each storage device. It increases energy storage and delivery capacity, ensuring it is dependable, active, and effective in various conditions [34, 35]. By utilizing intelligent energy flow balancing and keeping the battery and supercapacitors within their specified SOC ranges, the system maximizes energy economy and improves overall system performance [36, 37]. Each energy storage device in this design contains a bidirectional DC-DC converter to measure and compare system frequencies, hence improving the controllability and resilience of charge/discharge processes. Higher prices are a drawback, but overall savings should outweigh this. The battery can be charged while the supercapacitor is discharged thanks to separate bidirectional DC-DC converters. The controller detects three frequencies related to the grid: minimum permissible frequency (F_{min}), maximum acceptable frequency (F_{max}), and measured frequency (F_{mean}). Assume the reference frequency is 60Hz, 59Hz, and 61Hz for $Fief$, respectively. When the logic conditions are satisfied, the reference signal and the error signal generated by the PI block's comparator are routed. The switches are adjusted to carry out the intended charge/discharge operations [38]. An expansion of the classical PID controller is the fractional PID controller. Changes in the parameters of a controlled system and its controller have with a lesser impact on fractional-order controllers. It is easy to achieve iso-damping with a fractional-order controller. This fractional PID controller's generalized transfer function is provided in Eq.(32):

$$C(s) = \frac{U(s)}{E(s)} = K_P + \frac{K_I}{S^{\lambda}} + K_D S^{\mu}, and\ (\lambda, \mu \geq 0) \quad (32)$$

where C(s) is the output of the controller, U(s) is the signal due to control, E(s) is the signal of error , K_P is the gain of the proportional constant, K_I is the integration constant gain, K_D is the gain of the derivative constant, λ is the integration order, and μ is the differentiator order. The total harmonic distortion (THD) given by Eq.(33):

$$THD_{DC-DC\ Converter} = \frac{\sqrt{V_2^2+V_3^2+V_4^2+\cdots}}{V_1} \quad (33)$$

where $THD_{DC-DC\ Converter}$ is the total harmonic distortion for DC-DC converters,V_n is the RMS voltage of the harmonics. The complete block diagram of our proposed system is summarized in Fig.6. A promising method for controlling HES devices that combine batteries and supercapacitors is FOPID control. The potential advantages of dynamic reaction, stability, and battery longevity make it a tempting option for additional study, even though implementation requires careful thought. It may create a HESS that uses both batteries and supercapacitors, making it more responsive and efficient by combining FOPID control with a well-designed EMS.

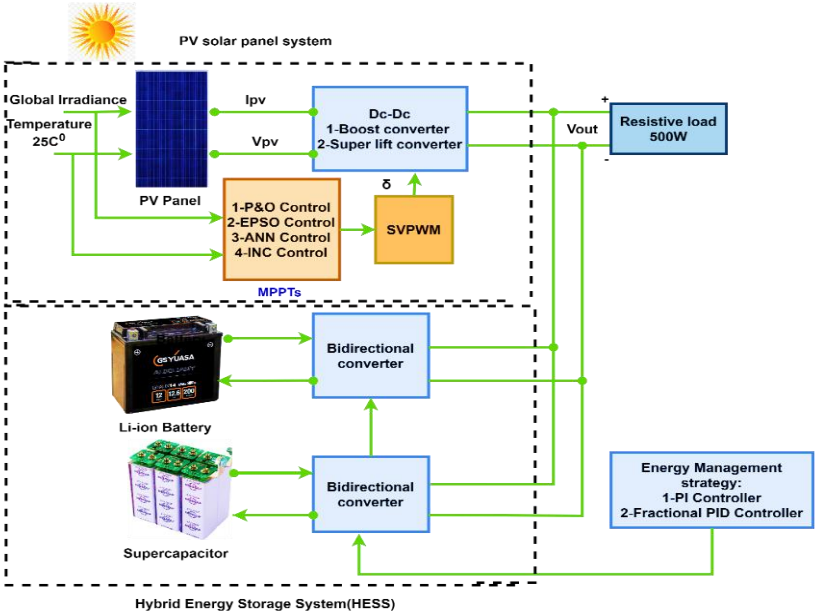

Fig. 6 Proposed Hybrid Energy Storage System.

3.RESULTS AND DISCUSSION

3.1.Performance of DC converters

The proposed system depicted in Figure 6 has been numerically simulated using MATLAB Simulink environment R2022b with a power sim library at sampling time bounded (%5Mse-10Mse). The simulation time is limited to (0 hr-3 hr), which presents all irradiance scenarios. Fig. 7 displays the P-V and V-I properties of the PV module at various levels of solar radiation.

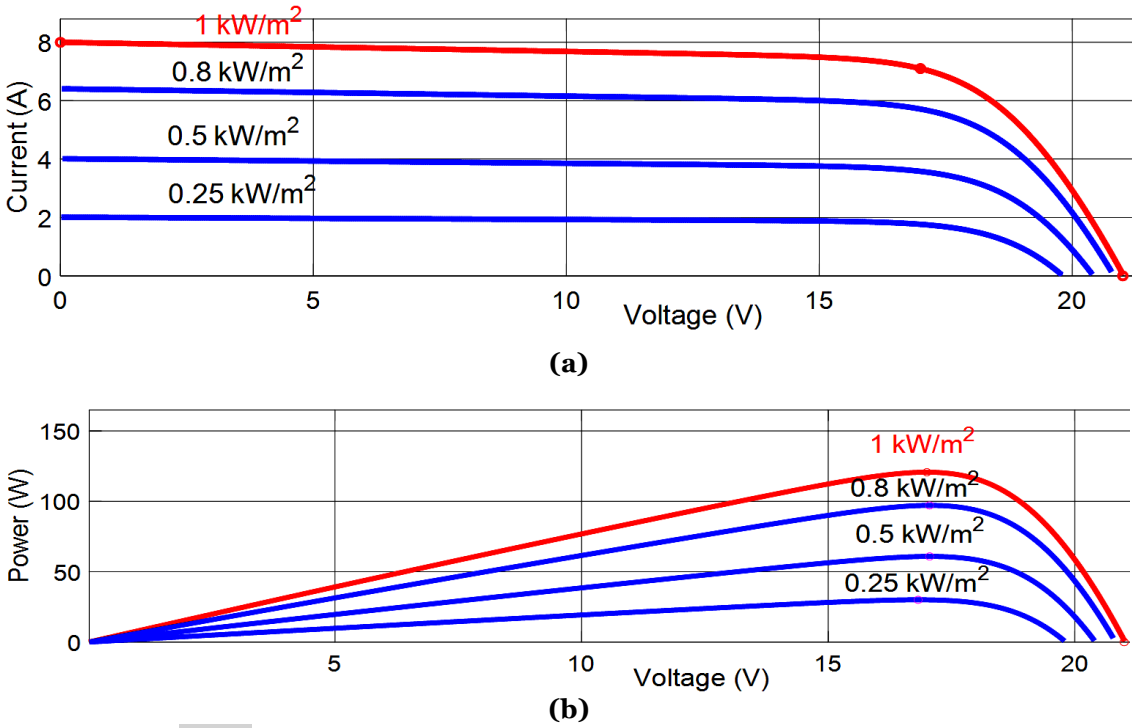

Fig. 7 PV Solar Panel Characteristics (A)I_V Curve (B)P_V Curve.

The tuning parameters of the proposed system are given in Table 5.

Table 5 Controllers' Parameter Values in HESS.

Parameter	Value
$K_p, K_i, K_d, \lambda, \mu$	1.477, 3077,0,110,55
Battery charge PI controller (K_p, K_i)	0.043,0.65
Supercapacitor PI controller (K_p, K_i)	0.45,14800
P&O (D_{old},V_{old},P_{old})	0.35,17,120
EPSO(C)	244

The operation of a boost and super lift Luo circuit is used to calculate a circuit's efficiency from the input/output power ratio. The load resistors chosen vary by 5 Ω. This test exploits the PV module's input sources. The simulation results are given in the figures below. The temperature of the PV system is 25C°. As shown in Fig. 8(A), the irradiance ranges from 6 to 18 hours. Thus, the simulation used in this work will depend on this region.

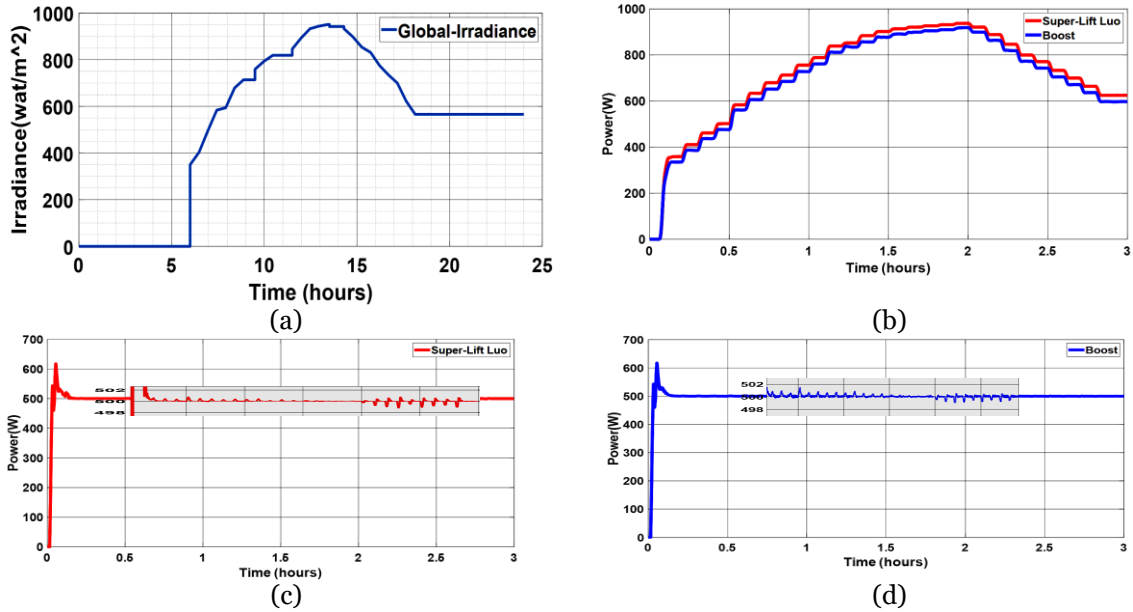

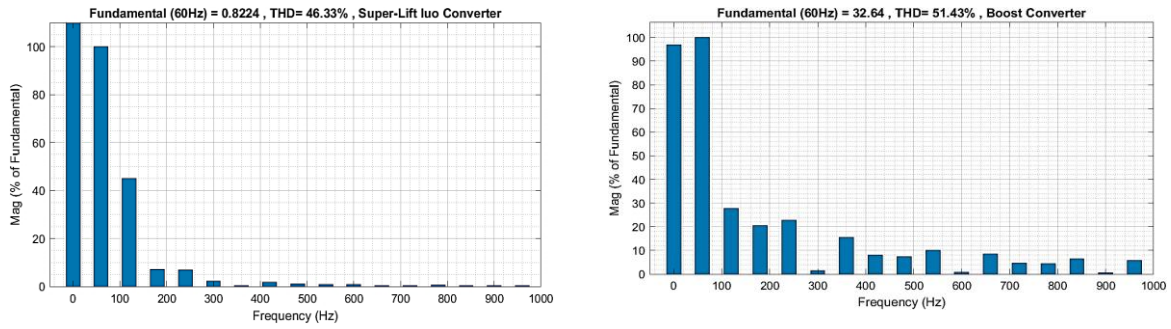

(e) **(f)**

Fig. 8 Boost and Super Lift - Luo Converters with Load (500W): (A) Solar Radiation Profile (B) Input PV Tracked Power (C) Super Lift Luo Converter Output Power. (D)Boost Converter Output Power (E) THD of the Boost and (F). Super Lift Luo Converter's Output Voltage.

As seen below in Figs. 8 (E and F), the THD voltage for both converters that satisfied the super lift Luo load condition was less than 1%, as required by IEEE standards. The Super Lift Luo converter's design includes additional circuitry that helps shape the input voltage waveform into a closer approximation of a sine wave, which explains why. THD is lowered as a result, as is the harmonic content. In contrast, the boost circuit's THD varies between 15% and 10%. The super lift Luo circuit with HESS offers higher, smoother performance and a potential advantage in reduced THD compared to a boost converter. The voltage gain of the Super Lift Luo circuit is substantially more significant. It uses a more complex circuit with capacitors and an extra inductor to achieve this. That allows increasing the output voltage significantly, often several times the input value.

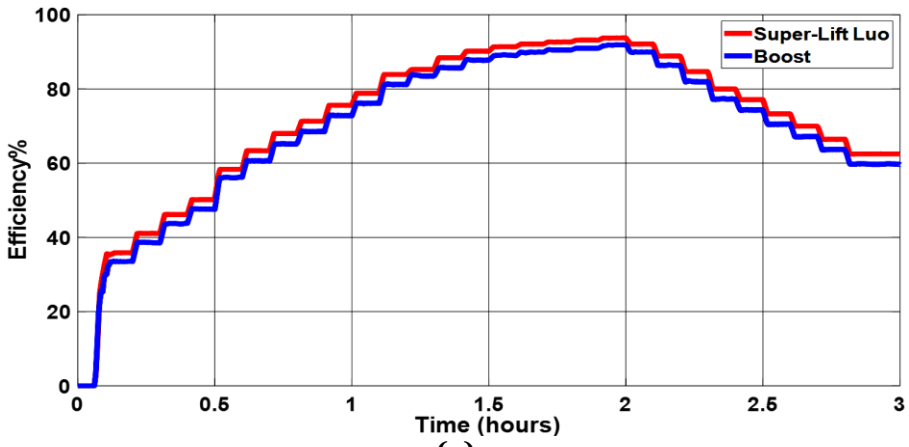

(a)

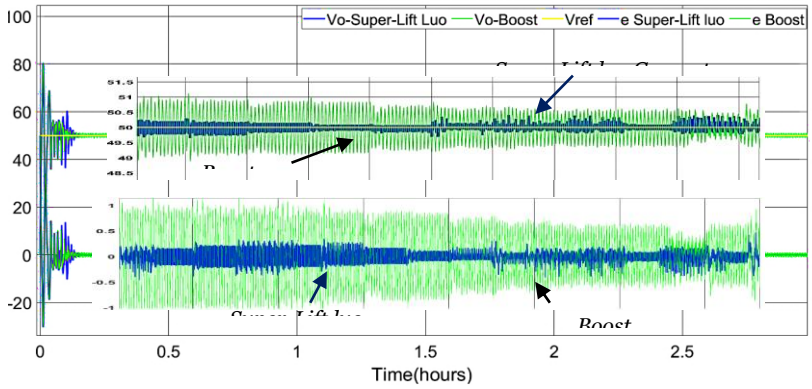

(b)

Fig. 9 Boost and Super Lift-Luo Converters with :(A) Terminal Voltage-Based Reference DC Voltage (50V) with their Errors(B) The DC-DC Converters' Efficiency.

Super Lift Luo converters can achieve higher efficiency, especially at low irradiance, due to their lower duty cycle, as seen in Fig.9(A). Because a high duty cycle is required for high voltage gain, the boost converter's efficiency decreases at low irradiance. However, efficiency increases with higher irradiance. That improves the system's reliability when the super lift Luo converter is used. As shown in Fig.9(B), under global irradiance or changing daily light intensity, the Super Lift Luo converter offers PV systems with MPPT several advantages.

Compared to a conventional boost converter, it can handle a broader range of input voltages, achieve higher efficiency, and increase MPPT performance. It is challenging to operate a PV panel under global irradiation. However, the Super Lift Luo converter consistently produces higher output power and lower overshoot than a boost converter to meet the desired load (500W). Super lift Luo converters have extra filtering components to provide a shallow ripple. Compared with a well-designed boost converter with appropriate filtering, Luo converters can deliver a smoother output voltage. The effect of both converters, when connected with the battery and SC that make up the (HESS) is seen in Fig.10. With the Super Lift Luo converter, the HESS can extract more power from the supercapacitor and battery, even in situations where the solar energy input varies due to the global irradiance, this is because energy losses during the conversion process are minimized by the super-lift Luo converter design.

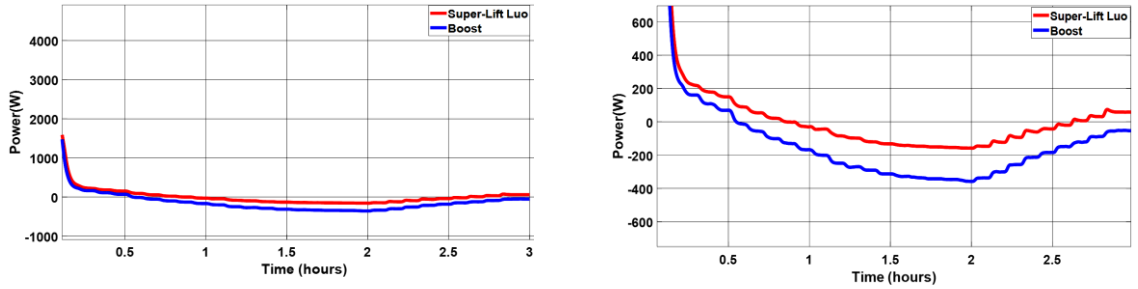

(a) (b)

Fig. 10. Effect of Boost and Super Lift Luo Converter with (A) Battery Output Power and (B) SC Output Power.

Figure 11 illustrates the impact of the two converters on the charging and discharging processes of the EMS, which comprises a rechargeable battery and supercapacitor. It is evident that when utilizing a super lift Luo, the battery's state of charge is approximately 0.2% greater than when using a boost converter. Additionally, super lift Luo is higher for supercapacitors, reaching 0.4% more significantly than a boost converter. The battery and supercapacitor can be charged faster and more efficiently due to the HESS with a super-lift Luo converter's higher efficiency and power output.

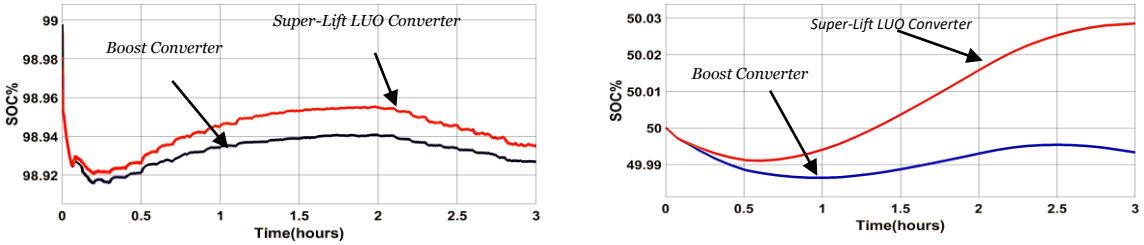

(a) (b)

Fig. 11 Effect of Boost and Super Lift Luo Converters on (A) Battery SOC and (B) Supercapacitor SOC.

3.2.Performance of MPPT Tracking Algorithm

This subsection will focus on the comparative outcomes of MPPTs in various scenarios. The MPP reached by every algorithm will determine the result of this study. The scenarios are based on an irradiance of 1000(W/m2), 400 (W/m2), a combination of 1000 - 400 (W/m2), and finally, global irradiance, and the results are shown in Fig.12 below.

Fig. 12 Maximum Power Tracked under (A) 1000 (w/m^2) ,(B) 400(W/m^2), (C) 1000-400 (W/m^2), (D)Maximum Extended Power under Global Irradiance Profile.

Depending on how radiation input affects the MPPT module's power, it is clear that the power output decreases with decreasing irradiation. When comparing the outcomes of the four algorithms, Perturb and observe(P%O) is a more considerable output power than the techniques and a higher value for current and constant voltage. Based on Fig.12(A), the P&O, ANN, EPSO, and InC algorithms can adjust the power points for different radiation sources.

Compared to another method, the P&O has shown the ability to perform MPPT under varying irradiation levels and to reach a stable point more quickly. The P&O technique can be used to get a module of 1kW. Compared to other algorithms, this outcome better affects the charging mode, providing greater power to P&O for charging and discharging, as Fig. 12(B) illustrates. However, for 400(W/m²), the INC is more accurate at tracking and requires less power than other algorithms. The particular reason for Inc MPPTs is that they employ advanced algorithms and enhanced perturbation control to overcome the drawbacks of conventional MPPT methods in low-irradiance scenarios. For this reason, it is used for MPP in areas with low solar irradiance. The P&O is more efficient and has the best MPP among PV panels regarding global irradiation. The following things may be the cause of the disparity. The specifications of the Simulink Lithium-ion battery model differ from those of the actual Li-ion battery Gel. Given the current integration time and capacity constraints, the SoC calculation for the Simulink model uses the battery voltage as a starting point. Simulink's battery model never simulates an aging or capacity-derated battery; instead, it always runs under new conditions.

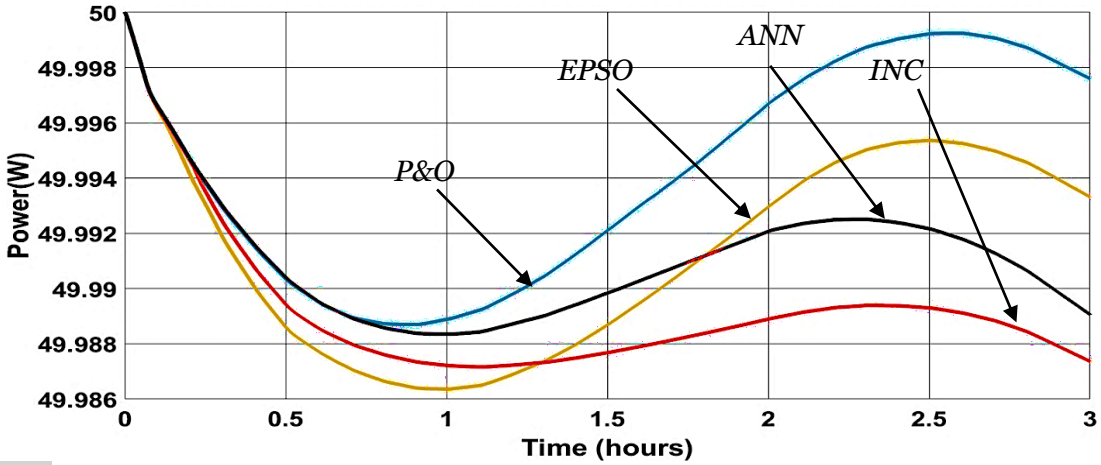

Fig. 13 Battery State of Charge with Different Algorithms: P&O, ANN, EPSO, and INC.

A greater power output from the P&O solar panel means more power is available for battery charging. It immediately quickens the rate at which the battery's SoC changes. Figure 13 illustrates that compared to other MPPT algorithms, P&O can improve battery SOC faster, especially in situations with global irradiation. Figure 14 shows the result, indicating that the supercapacitor will withstand an abrupt overload, preventing damage to the battery and shortening its lifespan. It is seen that the supercapacitor prevents a sudden overshoot in the load current, which reaches 400 W. The state of charge for SC will first decline from (99 - 98.14) % and deliver power to the load, as indicated by the figures below, and then the battery will provide the load with the appropriate amount of energy. In deceleration mode, the hybrid electric vehicle (HEV) can also use the SC to recover regenerative braking energy, initially for battery charging. Figure 14 displays the battery and SC EMS based on fractional PID. The scenario of (1000-400W/m^2).

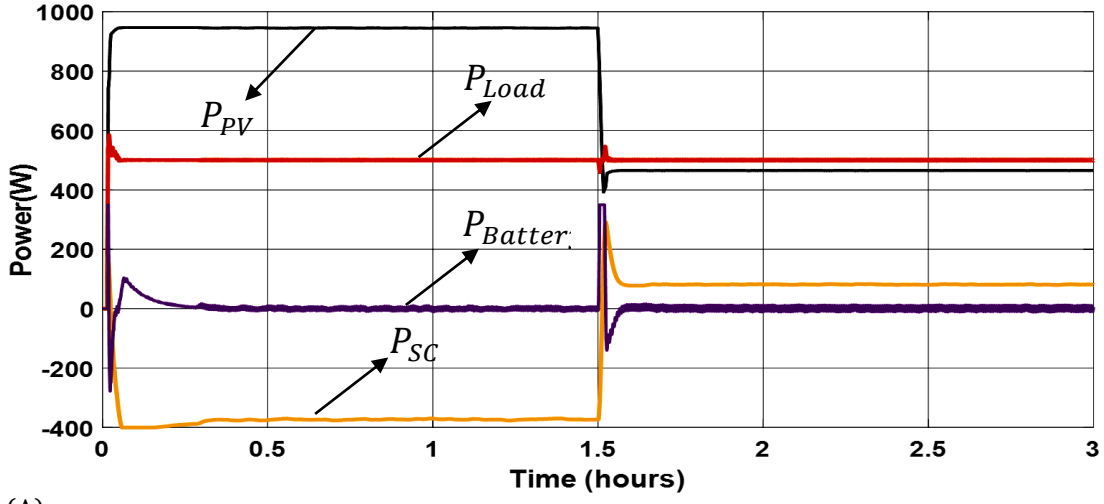

(A)

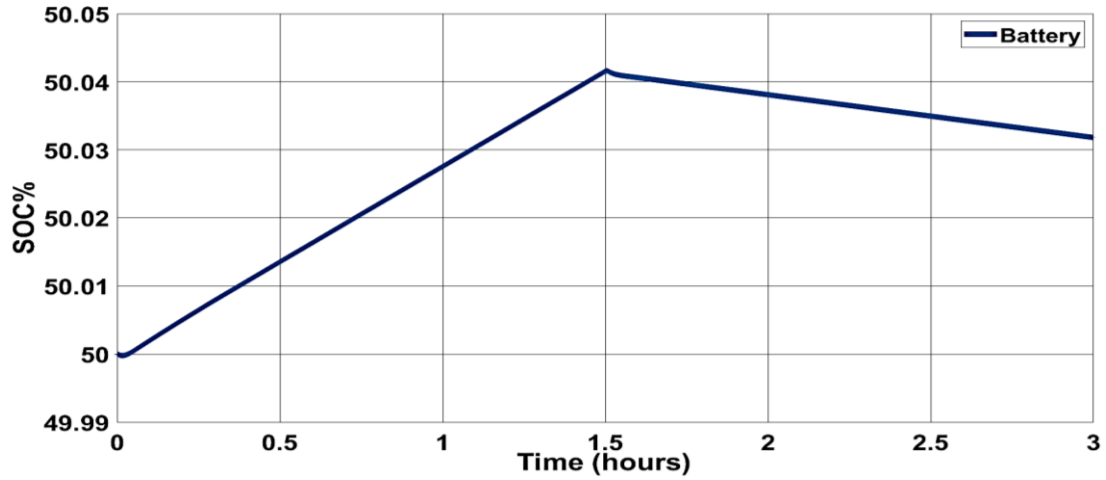

(B)

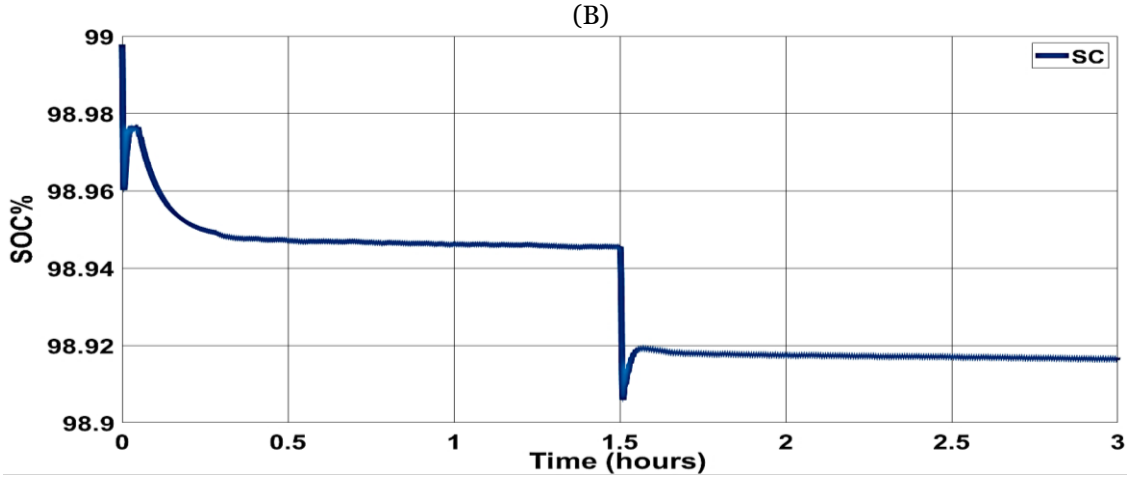

(c)

Fig. 14 Performance of the EMS under 1000-400 (W/m^2). (A) Outputs Power (B) SOC of the Battery (c) SOC of SC.

4.CONCLUSIONS

The Super lift Luo converter's performance over the classical boost converter is primarily due to its unique topology. This topology allows a higher boost ratio without compromising efficiency, making it ideal for applications that require a significant voltage step-up. Moreover, the Super lift Luo converter exhibits better transient response and reduced ripple, improving overall system performance. Efficient energy management is essential to maximizing system dependability and efficiency. The system can maximize energy storage and efficiency by carefully regulating energy flow between the solar panels, the battery, and the supercapacitor. It is especially crucial for grid-connected systems, as the HESS can help stabilize the grid by supplying electricity during spikes in demand and absorbing excess energy during dips in demand. The simplicity and resilience of the P&O method are the reasons behind its continuous dominance in MPPT tracking. The program modifies the power converter's duty cycle to follow the most significant PowerPoint. The P&O algorithm is a common choice in many applications due to its simple implementation and dependable performance, even though alternative algorithms may offer more advanced approaches. For the battery to remain safe and long-lasting, proper management is necessary. The battery's lifespan can be significantly increased by avoiding overcharging and excessive discharging. The Super Lift Luo converter and P&O algorithm deliver a robust battery charge-control solution that helps shield the battery from harm and preserve its performance over time. Comparing the fractional-order PID controllers to conventional integer-order controllers reveals several benefits. More control performance and system stability are possible with fractional-order controllers because they offer greater flexibility in parameter adjustment. Fractional-order derivatives allow the controller to behave more complexly, increasing tracking precision and robustness to disturbances. Supercapacitors' high power density and fast response time make them ideal for managing abrupt changes in load. Supercapacitors can assist in buffering the battery's load, reducing excessive current spikes, and enhancing system stability by swiftly absorbing and releasing energy. It is especially crucial for applications such as electric vehicles that experience frequent load swings.

ACKNOWLEDGMENTS

The researchers sincerely appreciate the University of Kerbala's staff for their guidance, support, and helpful critique of this study.

NOMENCLATURE

C	Capacitor in (μf)
E	Voltage source in (V)
G	Solar Irradiance in (W/m^2)
G_s	Voltage gains in (V)
I	Current in (A)
I_{bat}	Battery current in (A)
I_{sh}	Current resistance in (A)
L	Inductance in (mH)
P_{batt}	Power of the battery
P_N	Nominal power of the PV panel in (W)
P_{Sc}	Power of SC in W
R_{bat}	Battery resistance in (Ω)
R_{SC}	Supercapacitor stack capacitor.
T	Temperature, ℃
V_{bat}	Battery voltage in (V)
Greek symbols	
δ	Duty cycle

REFERENCES

[1] Murali S, Panda KP, Panda G. **PV-HESS Fed BLDC Driven Water Pumping System with PSO-Based MPP Tracking Employing Zeta Converter.** *International Conference on Innovative Smart Grid Technologies (ISGT Asia)* 2018; Singapore: 196–201.

[2] Gonzalez-Castano C, Restrepo C, Kouro S, Rodriguez J. **MPPT Algorithm Based on Artificial Bee Colony for PV System.** *IEEE Access* 2021; **9**: 43121–43133.

[3] Aurairat A, Plangklang B. **An Alternative Perturbation and Observation Modifier Maximum Power Point Tracking of PV Systems.** *Symmetry* 2022; **14**(1): 186.

[4] Abdellatif WSE, Mohamed MS, Barakat S, Brisha A. **A Fuzzy Logic Controller-Based MPPT Technique for Photovoltaic Generation System.** *International Journal on Electrical Engineering and Informatics* 2021; **13**(2): 394–417.

[5] Gupta AK, Pachauri RK, Maity T, Chauhan YK, Mahela OP, Khan B, et al. **Effect of Various Incremental Conductance MPPT Methods on the Charging of Battery Load Feed by Solar Panel.** *IEEE Access* 2021; **9**: 90977–90988.

[6] Pilakkat D, Kanthalakshmi S, Navaneethan S. **A Comprehensive Review of Swarm Optimization Algorithms for MPPT Control of PV Systems under Partially Shaded Conditions.** *Electronics* 2020; **9**(3): 434.

[7] Ali MN, Mahmoud K, Lehtonen M, Darwish MMF. **Promising MPPT Methods Combining Metaheuristic, Fuzzy-Logic, and ANN Techniques for Grid-Connected Photovoltaic.** *Sensors* 2021; **21**(4): 1244.

[8] Cherusseri J, Pandey D, Thomas J. **Symmetric, Asymmetric, and Battery-Type Supercapacitors Using Two-Dimensional Nanomaterials and Composites.** *Batteries & Supercaps* 2020; **3**(9): 860–875.

[9] Zhang Z, Ding T, Zhou Q, Sun Y, Qu M, Zeng Z, et al. **A Review of Technologies and Applications on Versatile Energy Storage Systems.** *Renewable and Sustainable Energy Reviews* 2021; **148**: 111263.

[10] Wen J, Zhao D, Zhang C. **An Overview of Electricity Powered Vehicles: Lithium-Ion Battery Energy Storage Density and Energy Conversion Efficiency.** *Renewable Energy* 2020; **162**: 1629–1648.

[11] Sulzer V, Mohtat P, Aitio A, Lee S, Yeh YT, Steinbacher F, et al. **The Challenge and Opportunity of Battery Lifetime Prediction from Field Data.** *Joule* 2021; **5**(8): 1934–1955.

[12] Natarajan S, Ulaganathan M, Aravindan V. **Building Next-Generation Supercapacitors with Battery Type Ni(OH)2.** *Journal of Materials Chemistry A* 2021; **9**(28): 15542–15585.

[13] Radhika S, Margaret V. **A Review on DC-DC Converters with Photovoltaic System in DC Micro Grid.** *Journal of Physics: Conference Series* 2021; **1804**(1): 012015.

[14] Sutikno T, Samosir AS, Aprilianto RA, Purnama HS, Arsadiando W, Padmanaban S. **Advanced DC-DC Converter Topologies for Solar Energy Harvesting Applications: A Review.** *Clean Energy* 2023; **7**(3): 555–570.

[15] Sarvi M, Azadian A. **A Comprehensive Review and Classified Comparison of MPPT Algorithms in PV Systems.** *Energy Systems* 2022; **13**(2): 281–320.

[16] Ali MHM, Mohamed MMS, Ahmed NM, Zahran MBA. **Comparison Between P&O and SSO Techniques Based MPPT Algorithm for Photovoltaic Systems.** *International Journal of Electrical and Computer Engineering* 2022; **12**(1): 32–40.

[17] Abouadane H, Fakkar A, Sera D, Lashab A, Spataru S, Kerekes T. **Multiple-Power-Sample Based P&O MPPT for Fast-Changing Irradiance Conditions for a Simple Implementation.** *IEEE Journal of Photovoltaics* 2020; **10**(5): 1481–1488.

[18] Hayder W, Ogliari E, Dolara A, Abid A, Hamed MB, Sbita L. **Improved PSO: A Comparative Study in MPPT Algorithm for PV System Control under Partial Shading Conditions.** *Energies* 2020; **13**(8): 2035.

[19] Firdaus AA, Yunardi RT, Agustin EI, Nahdliyah SDN, Nugroho TA. **An Improved Control for MPPT Based on FL-PSO to Minimize Oscillation in Photovoltaic System.** *International Journal of Power Electronics and Drive Systems* 2020; **11**(2): 1082–1087.

[20] Gündoğdu A, Çelikel R. **ANN-Based MPPT Algorithm for Photovoltaic Systems.** *Turkish Journal of Science and Technology* 2020; **15**(2): 101–110.

[21] Rahman MM, Islam MS. **PSO and ANN Based Hybrid MPPT Algorithm for Photovoltaic Array under Partial Shading Condition.** *Engineering International* 2020; **8**(1): 9–24.

[22] Ali MN, Mahmoud K, Lehtonen M, Darwish MMF. **An Efficient Fuzzy-Logic Based Variable-Step Incremental Conductance MPPT Method for Grid-Connected PV Systems.** *IEEE Access* 2021; **9**: 26420–26430.

[23] Padhee S, Pati UC, Mahapatra K. **Design of Photovoltaic MPPT Based Charger for Lead-Acid Batteries.** *IEEE International Conference on Emerging Technologies and Innovative Business Practices for the Transformation of Societies (EmergiTech)* 2016; Mauritius: 351–356.

[24] Yunus Khan TM, Soudagar MEM, Kanchan M, Afzal A, Banapurmath NR, Akram N, et al. **Optimum Location and Influence of Tilt Angle on the Performance of Solar PV Panels.** *Journal of Thermal Analysis and Calorimetry* 2020; **141**(1): 511–532.

[25] Hamad AA, Khalf MF, Abdoon FM, Thivagar ML. **Analysis of Dynamic Systems Through Artificial Neural Networks.** *Tikrit Journal of Engineering Sciences* 2024; **31**(2): 148–158.

[26] Zhou W, Zheng Y, Pan Z, Lu Q. **Review on the Battery Model and SOC Estimation Method.** *Processes* 2021; **9**(9): 1685.

[27] Cultura AB, Salameh ZM. **Modeling, Evaluation, and Simulation of a Supercapacitor Module for Energy Storage Application.** *International Conference on Computer Information Systems and Industrial Applications (CISIA)* 2015; Bangkok, Thailand: 876–882.

[28] Shenbagalakshmi R, Vijayalakshmi S. **Analysis of Super Lift Luo Converter with Discrete-Time Controller.** *Sadhana* 2020; **45**(1): 1–5.

[29] Arunkumar N, Sivakumaran TS, Ramashkumar K, Shenbagalakshmi R. **Analysis, Modeling and Simulation of State Feedback Control for Positive Output Super Lift Luo Converter.** *Circuits and Systems* 2016; **7**(11): 3971–3983.

[30] Zongo OA. **Comparing the Performances of MPPT Techniques for DC-DC Boost Converter in a PV System.** *Walailak Journal of Science and Technology* 2021; **18**(2): 9152.

[31] Balasubrahmanyam CS, Gupta OH. **Detailed Study of Solar Energy Conversion System Using Boost Converter—A New MPPT Technique.** *Journal of The Institution of Engineers (India): Series B* 2020; **101**(6): 631–639.

[32] Basha CH, Rani C. **Different Conventional and Soft Computing MPPT Techniques for Solar PV Systems with High Step-Up Boost Converters: A Comprehensive Analysis.** *Energies* 2020; **13**(2): 371.

[33] Rajasekaran R, Rani PU. **Bidirectional DC-DC Converter for Microgrid in Energy Management System.** *International Journal of Electronics* 2020; **108**(11): 1894–1915.

[34] Punna S, Manthati UB. **Optimum Design and Analysis of a Dynamic Energy Management Scheme for HESS in Renewable Power Generation Applications.** *SN Applied Sciences* 2020; **2**(3): 483.

[35] Cabrane Z, Kim J, Yoo K, Ouassaid M. **HESS-Based Photovoltaic/Batteries/Supercapacitors: Energy Management Strategy and DC Bus Voltage Stabilization.** *Solar Energy* 2021; **216**: 551–563.

[36] Zhang Q, Wang L, Li G, Liu Y. **A Real-Time Energy Management Control Strategy for Battery and Supercapacitor Hybrid Energy Storage Systems of Pure Electric Vehicles.** *Journal of Energy Storage* 2020; **31**: 101721.

[37] Elmorshedy MF, Elkadeem MR, Kotb KM, Taha IBM, Mazzeo D. **Optimal Design and Energy Management of an Isolated Fully Renewable Energy System Integrating Batteries and Supercapacitors.** *Energy Conversion and Management* 2021; **245**: 114584.

[38] Ammari C, Belatrache D, Touhami B, Makhloufi S. **Sizing, Optimization, Control and Energy Management of Hybrid Renewable Energy System—A Review.** *Energy and Built Environment* 2022; **3**(4): 399–411.